DEVELOPMENT AND TESTING OF ELECTRIC AND ADVANCED PROPULSION SYSTEMS AT TU DRESDEN

M. Tajmar*, D. Bock, F. Nürmberger, A. Hock, and M. Kössling
Institute of Aerospace Engineering, Technische Universität Dresden, Germany

Abstract

The institute of aerospace engineering at TU Dresden is developing a number of electric propulsion thrusters in the low power range for micro and small satellites as well as for precision pointing science applications. The first concept is a FEEP thruster called NanoFEEP using gallium as propellant that is small enough to be integrated into a CubeSat enabling formation flying and orbit control on a widely available small satellite platform. Also the power requirement is so small that up to 8 thrusters can be fired simultaneously enabling full 3-axis attitude and orbit control with maximum thrusts in the range up to 10 µN. The second concept uses gas as propellant using a porous MEMS silicon chip with carbon nanotubes for field ionization. The thruster requires only a single power supply with a few hundred volts DC and no magnetic field. A first prototype of the MEMS ion thruster demonstrated a thrust level of 150 µN with a chip size of only 25 mm. Due to its carbon nanotube array it can work also with AC voltages and acts as its own neutralizer. In order to complement our education program on electric propulsion, a low power hall thruster together with a cathode is also currently under development by students aiming at the 50-150 W range. All thrusters can be tested on a new torsion thrust balance that promises thrust resolutions down to the Nano-Newton range. In addition to classical electric propulsion, we are also working on very advanced propellantless propulsion concepts which are briefly introduced.

1. INTRODUCTION

Small- and Pico-Satellites ("CubeSats") are becoming increasingly popular especially within the education community as they enable to design and actually build a complete satellite with students. These satellites are constantly improving their capabilities – however up to now propulsion for attitude and ever more orbit control is a real challenge.

At TU Dresden, we are developing highly miniaturized electric propulsion systems that shall enable onboard propulsion for small satellites are well as providing precision thrust for scientific missions e.g. to enable highly demanding formation flying[1]. A core focus of our activities is the development of field emission thrusters. Our so-called NanoFEEP thruster[2-4] uses liquid metal propellant and is so compact that it can be integrated within the rails at the edge of CubeSats. We are also developing a gas-fed field ionization thruster[5] that is highly scalable and allows both ion and electron emission with the same chip that allows thrusts in the 100s of µN. Even larger is a low-power Hall thruster[6] that is presently under development that enables thrusts in the mN range. In order to complement our electric propulsion thrusters, we are also developing a thrust balance[1] with a resolution in the nN range.

Our group is also actively looking at future and very advanced (potentially) propellantless propulsion systems. This paper is briefly summarizing our latest electric propulsion as well as breakthrough propulsion activities.

2. MICRO ELECTRIC PROPULSION

2.1. Highly Miniaturised Field Emission Thruster (NanoFEEP)

Field emission thrusters (FEEP) are ideal for miniaturization as only a single high voltage power supply is required. It usually concists of a needle or capillary that is wetted with a liquid metal propellant. Then a very high electric field is applied between the tip and an extractor electrode and ions are directly pulled out of the liquid metal film and accelerated by the same field. This allows a very compact design, especially if the propellant is a liquid metal that is stored in a small tank only working with capillary force feeding towards the emission site.

2.1.1. Thruster Design of NanoFEEP

With respect to the limitations of available power and weight on a CubeSat, our main goals in the thruster design were miniaturization and power efficiency. A cut away view of our NanoFEEP module is shown in Fig. 1. To achieve a highly efficient and stable ionization we use our novel porous Liquid Metal Ion Source (LMIS) which consists of a very sharp, electrochemically etched porous tungsten needle and a tantalum reservoir filled with the metal propellant. The open porosity of the tungsten needle provides capillary forces, which hold the liquid metal propellant at the needle tip, and enables self-feeding propellant flow during operation. Thus, no valves or propellant feeding devices are required.

* Director of Institute, Head of Space Systems Chair, Email: martin.tajmar@tu-dresden.de

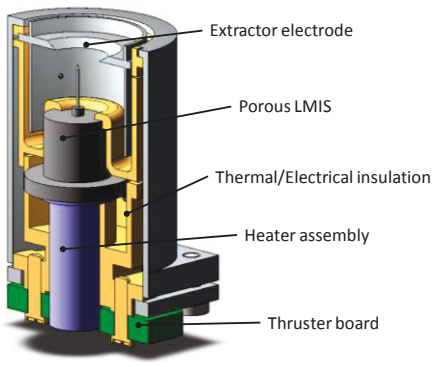

Fig. 1 Cut away view of the NanoFEEP model

Fig. 2 Manufactured, highly miniaturized NanoFEEP thruster; Thruster size compared to a 1 € coin

The porous LMIS is heated up by the heater assembly and is supported by thermal and electrical insulations which shape is optimized by thermal simulations to minimize thermal losses. With this thermal optimization of the thruster geometry, only 50 to 90mW of heating power (depending on satellite structure temperature) are necessary to keep the propellant liquid at a temperature of 50°C. Furthermore gallium with its low melting temperature of approximately 30°C is used as propellant to keep down the power demand for melting the propellant compared to commonly used propellants, like Indium with a melting temperature of 157°C.

To avoid short circuits between the LMIS on high voltage potential and the extractor electrode during long term operation the NanoFEEP module features labyrinth shielding. Thus, possible surface contamination of the inner insulation structure with the electrically conductive propellant caused by micro-droplets will not affect long term operation. The major reason for the given limit of operating time of approximately 1,800h is due to the used amount of propellant (0.25g gallium per thruster). This maximum operation time is thought to be sufficient for the first precursor mission, but it can be enhanced easily in future missions by using larger reservoirs of the LMIS. Though, the dimensions of the thruster would need to be adjusted in that case.

With the presented NanoFEEP design a field emission thruster could be miniaturized down to Ø13x21mm with a total weight of less than 6g and a volume of less than 3cm^3 per thruster. Fig. 2 shows one manufactured NanoFEEP thruster compared to a one Euro coin to visualize the thruster size. A further miniaturization of the thruster is currently under investigation as saving only a few Millimeters in size would strongly simplify the thruster integration in a 1U-CubeSat.

2.1.2. Thruster Performance

First tests were performed to determine the functionality of the miniaturized thruster design and to roughly characterize the thruster performance. As it can be seen in Fig. 4, stable operation of the thruster with the novel porous LMIS running with gallium propellant could be demonstrated indicated by the characteristic violet light emission at the needle tip.

A typical current-voltage characteristic (begin of life) of a NanoFEEP thruster is shown in Fig. 4. NanoFEEP typically starts operating at a voltage between 3.3 and 4kV, begin of life. The starting voltage increases with operation time to approximately 6 to 7kV while the slope of the current-voltage characteristic, in other words the impedance, decreases. Considering this typical behavior of FEEP thrusters with needle emitters and adding a safety margin to the required voltage range, a high voltage demand of 12kV is defined as maximum for the required power processing unit. NanoFEEP was tested up to an emission current of 250µA which corresponds to a thrust of approximately 22µN without any problems. This emission current limit of 250µA is due to the specified maximum available output current of the high voltage converter which shall be used on the CubeSat platform. However, a maximum emission current of 100µA corresponding to a thrust of approximately 8µN is recommended for long term operation (more than a hundred hours) to prevent needle erosion.

Fig. 3 Operating NanoFEEP thruster

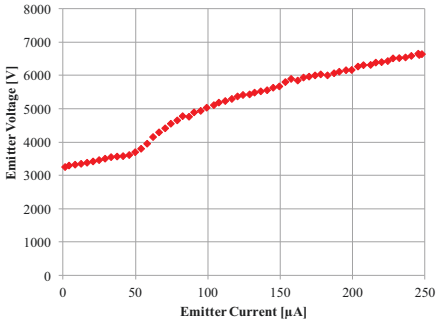

Fig. 4 Current-Voltage Characteristic of NanoFEEP

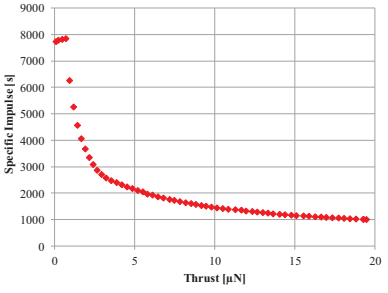

Fig. 5 Specific Impulse over Thrust Range of NanoFEEP

Additionally, tests were performed to determine the mass efficiency of the novel porous needle LMIS with gallium propellant used in the NanoFEEP thrusters. During these mass efficiency tests, the LMIS was operating at different constant emission currents and was weighed before and after each test run. Mass efficiency was then calculated by comparing the exhausted charge to the mass difference. The calculated mass efficiency showed the typical exponential decline with increasing emission currents. This decline is due to the increasing amount of unionized droplets at higher emission currents. For calculating the specific impulse of NanoFEEP as a function of thrust, shown in Fig. 5, the described mass efficiency as a function of emission current was used.

The generated thrust was calculated analytically using the measured emission current and assuming a constant beam divergence factor of 0.8. To verify the used analytic formulas for thrust and specific impulse it is planned to test the NanoFEEP thruster on our newly developed thrust balance5 in the near future. Besides measuring the generated thrust directly on a thrust balance, it is also planned to measure the spatial beam divergence of the NanoFEEP module as a function of thrust with a plume diagnostic facility, which is currently under development at TU Dresden.

Besides the mentioned performance tests a first engineering model of the power processing unit (PPU) for NanoFEEP was also tested[4]. This PPU was designed regarding the CubeSat specifications using off-the-shelve DC-to-HV-DC converter from EMCO (two AH60 models in series) to apply the required maximum high voltage of 12kV and the maximum current of 250µA. Through, analyses of the total power demand of this PPU showed a quite poor overall power converting efficiency of 14-28% depending on the applied thrust level. This low efficiency is due to the low power converting efficiency of the EMCO DC-to-HV-DC converter especially at low power output. Therefore TU Dresden is currently developing a completely new PPU in cooperation with a local electronics company (GBS Elektronik) with the goal to significantly increase the power converting efficiency of the PPU. This will significantly improve the possible thrust capabilities of NanoFEEP on a CubeSat with its strong power limitations.

We are currently working together with Würzburg university to implement the NanoFEEP thruster on the UWE satellite platform[2].

2.2. MEMS Gas Field Ionization Source (GFIS) Truster

The second field emission thruster which we are currently developing is a gas thruster using a porous MEMS silicon chip with carbon nanotubes (CNTs) for field emission. The gas is flowing along a CNT forest opposite of an extractor grid which generates the high electric field for ionization (see Fig. 6). In fact, so-called gas field ion sources (GFIS) are a relatively new research topic and are becoming more and more important as they are already replacing Liquid-Metal-Ion Sources in several applications. A Xenon-based GFIS would be a hybrid between a classical ion and field emission thruster without the use of magnetic fields and liquid propellants. Such a concept looks very appealing to be investigated for MEMS electric propulsion as it avoids the usual small electrode clogging lifetime issue completely. The lifetime critical factor in this design will be similar to the classical ion engines: due to ionization inefficiencies, neutral gas atoms will collide with fast beam ions and produce slow charge-exchange ions that can flow back and cause sputtering of grids and tips. A multi-grid structure with low voltages at the top is necessary to limit the backflow energies to a value below the sputter threshold. This has already been done for electron field emission sources. Another advantage is the fact that the CNT chip can emit both polarities (positive ions and negative electrons) depending on the polarity of the power supply which can eliminate the need for a separate neutralizer.

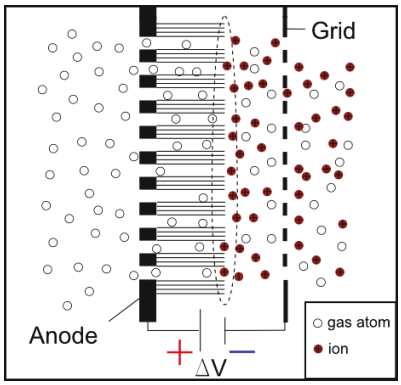

Fig. 6 MEMS Gas Field Ionization Source (GFIS) Thruster Concept

2.2.1. Novel manufacturing approach

Reviewing the newly introduced designs, several aspects showed further potential for significant improvement in performance of the ion source. The first aspect of our investigation was the carbon nanotube layer. As field ionization only occurs in the strong electric field region close to the CNT-tips, a high CNT-count and thus density is generally more advantageous. Though sparse CNT-growth improves the field enhancing properties and thus reduces the required voltage, it also limits the amount of generated ion current. This led to the goal to manufacture a flow through electrode with a denser and more uniform CNT-layer

Another aspect was the shape and fabrication of the porous substrate. As the hole-diameter drives the distance between the carbon nanotubes, and thus is supposed to be as small as possible for a maximum ion current, the design should have a significant lower hole-diameter. A potential alternative to dry etching of the porous substrate is laser drilling. The usage of laser drilling would enable easier alteration of shape parameters to investigate different arrangements, a less risky fabrication process and has the potential of generating smaller hole-diameters. As the manufacturing of such a structure through laser processing has not yet been investigated, it was chosen as the manufacturing process for the new substrates.

To be able to test the ion source in an open and closed architecture assembly, the case design was chosen to be modular, to easily adapt for different test procedures. To achieve these goals, we partnered up with experts in CNT deposition (Fraunhofer-Institut für Keramische Technologien und Systeme IKTS) and laser manufacturing (Laser Institute of the Hochschule Mittweida).

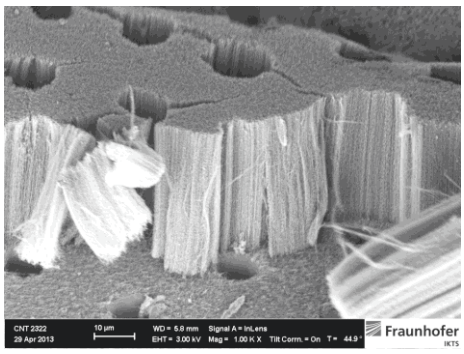

Fig. 7 Results of the Laser Drilling and CNT-Deposition

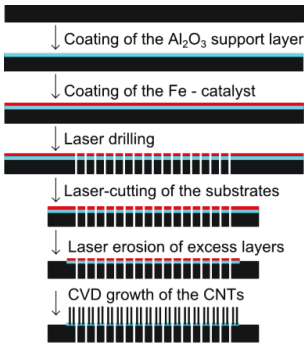

Fig. 8 Fabrication Process of the Flow Through Electrode

2.2.2. Fabrication process

As base material highly n-doped, 550 µm thick silicon wafers were obtained and the substrate size was set to be 26 mm in diameter with a 20 mm diameter region in the centre for the CNT-layer and the holes. The wafers were first coated by a sapphire, Al2O3 layer and afterwards with a Fe-catalyst layer. These layers are crucial for the CNT-deposition. The Al2O3 improves the overall quality of the deposition result, while the Fe-catalyst, consisting of nm-sized Fe-particles, defines the growth site for the carbon nanotubes.

We then chose to first perform laser drilling and afterwards CNT deposition in order to not damage CNTs during the production process. To minimize pollution of the coated surface and to minimize the achieved hole-diameter at the exit side, the drilling was performed through the back side of the wafers using a pulsed UV-laser. This was followed by the laser-cutting of the substrates and erosion of the excess layers. The laser drilling achieved hole-diameters as little as 10 µm with a maximum substrate transparency of 19% and a total of 450.000 holes drilled in average per substrate – achieving an aspect ratio of close to 50:1 as shown in Fig. 7.

After the laser processing, the substrates were handed to the IKTS institute where the CNTs were deposited using atmospheric pressure chemical vapour disposition, APCVD. This process involved the placement of the substrates inside an oven, which is filled with a carbonaceous gas. When heating up the oven to temperatures above 700°C, the gas molecules break apart resulting in free atomic carbon. Eventually, the carbon atoms settle around the Fe-particles forming tube like structures, carbon nanotubes. The resulting CNT-layers achieved a maximum CNT-length of 130µm with high density as well as close growth near the holes. Fig. 7 illustrates an angular view of the layer, with a section being whipped of for better vision. The whole fabrication process is shown in Fig. 8

In summary, the flow through electrode manufacturing generated very promising results, having achieved very small hole-diameters as well as high CNT-density and uniformity. In addition to the CNT-electrodes, the Laser Institute also manufactured grid electrodes to serve as cathodes. These were manufactured using similar laser processing parameters. The entire design of the first prototype can be seen in Fig. 9. It consists of a modularly designed PEEK case, copper contact electrodes, a Teflon pipe serving as gas supply and it can be altered for usage as an open and closed architecture ion source.

2.2.3. Test Results

While all preceding research work had focused on open architecture gas field ion sources, the new ion source was the first device capable of performing as a closed architecture ion source as well. Argon gas was chosen as the initial gas for all tests, because of its availability in the lab.To determine the field enhancement properties of the electrodes using the Fowler-Nordheim model, the first tests performed were electron emission tests at 10^{-6} mbar. The tests revealed an average field enhancement factor of the electrodes of 4000. The maximum currents achieved were 1mA, but to prevent early damage to the electrodes and the rest of the device, no higher electron currents were attempted, though are possible. The resulting I-V plot of one of the CNT electrodes is shown in Fig. 10.

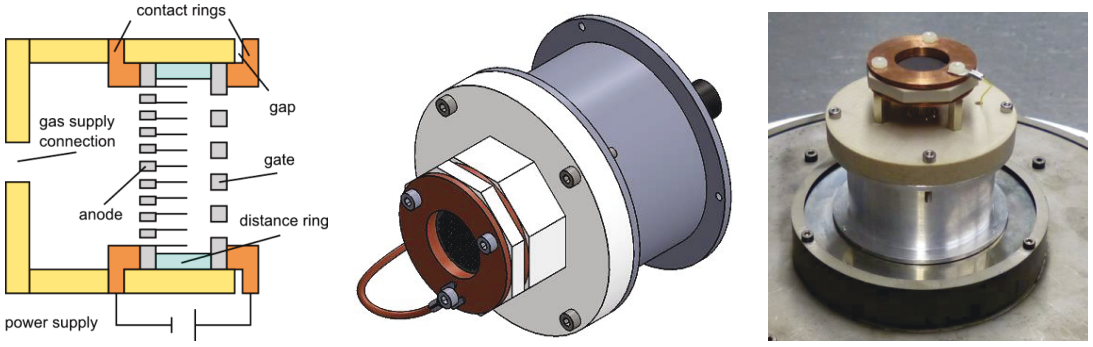

Fig. 9 Test Module Design and Actual Laboratory Model

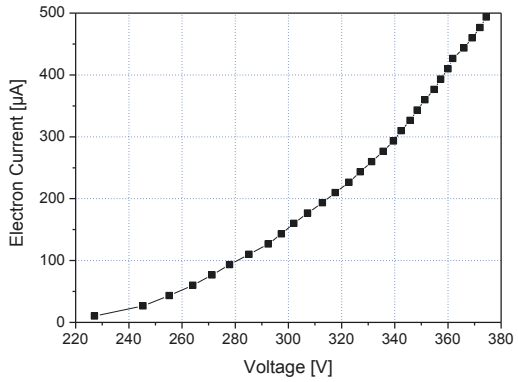

Fig. 10 Electron Emission Test Results

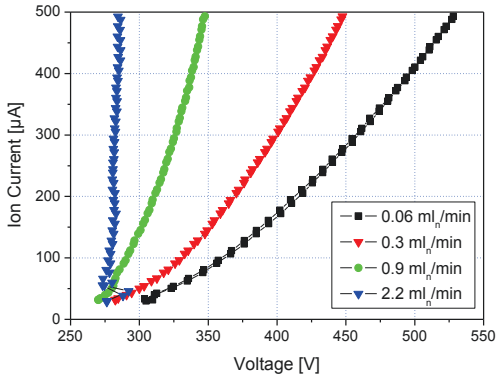

Fig. 11 Ion Emission Test Results with Argon at different Gas Flow Rates

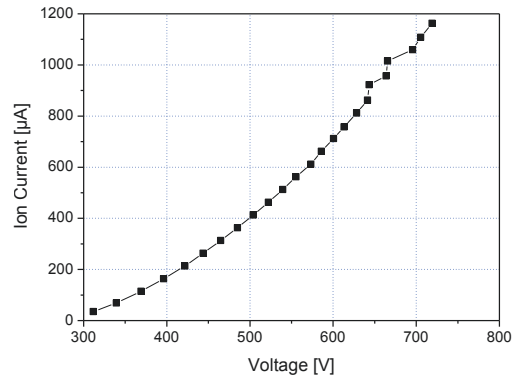

Fig. 12 Maximum achievable Current with Argon at 0.06 ml_n/min

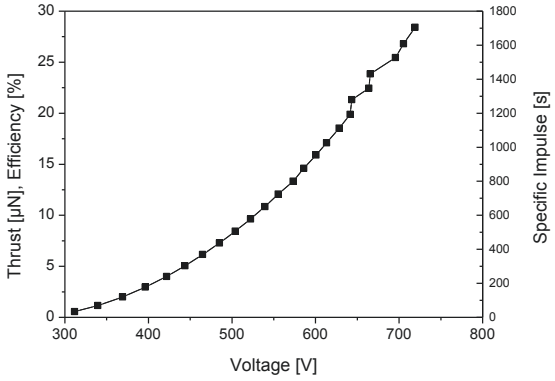

Fig. 13 Thruster-Related Performance Data of the MEMS GFIS Chip, flow rate: 0.06 ml_n/min Argon

By switching the polarity between the electrodes, the CNT electrode serves as an anode for field ionization. The field ionization tests were performed at different flow rates between 0.06 mln/min and 2.2 mln/min. As higher flow rate increases the probability of micro discharges inside the plasma generator, the ion source was operated at low voltages, as the first goal was to prove its functionality. The resulting I-V plot can be seen in Fig. 11.

Another aspect of interest was the maximum achievable ionization efficiency. The higher the used voltage, the more gas particles are being field ionized on their passage through the plasma generator. However, a higher voltage also increases the probability of micro discharges. Thus a maximum voltage can be determined below which no discharges appears. This maximum voltage was found to be 740 V at 0.06 mln/min. At this voltage, an ion current of 1.2 mA was achieved, which equals to an ionization efficiency of approximately 28%. The related I-V plot can be seen in Fig. 12 as well as the maximum achievable ion current at the lowest flowrate.

The thruster related performance data is shown in Fig. 13 for the lowest flow rate of 0.06 mln/min. A total thrust of close to 30 µN at a specific impulse of 1700 s could be achieved with a single chip active area of 20 mm diameter with this first prototype. The overall efficiency was also 30%. This is similar to the performance of FEEP thrusters but with a gas propellant. Different propellants like Xenon and higher voltages can easily create thrusts in the several hundred µN range similar to other µN ion thruster technologies like the µN-RIT. However this GFIS thruster concept requires only a single DC power supply, no magnetic fields and its thrust is highly controllable from µN to several hundred of µN. This makes it also a very interesting candidate for precise attitude and orbit control applications.

2.3. Low Power Hall Effect Thruster

A laboratory low-power Hall effect thruster with a boron nitride discharge chamber has been recently developed at the institute of aerospace engineering[6]. Its purpose is to investigate the performance in the region of 50-150 W. The thruster is provided with a solenoid in order to vary the magnetic field strength and thus to help finding the point of best operation (see Fig. 14). Additionally, a low-current lanthanum hexaboride hollow cathode for operation with the HET has been developed. It has been designed to provide a current of up to 1 A.

2.3.1. Design

For the production of the magnetic field, a concentric solenoid was chosen which is placed inside of the thruster between the center stem and the outer pole piece. Because of the small size of the thruster, it was decided to waive magnetic shields which in some thrusters help to improve the magnetic field and to produce a higher gradient. The discharge chamber wall material of choice became hexagonal boron nitride (BN) with calcium borate as binder. The anode is a ring-shaped disc, which easily can be substituted. Therefore, nonmagnetic steel has been chosen as anode material for first experiments.

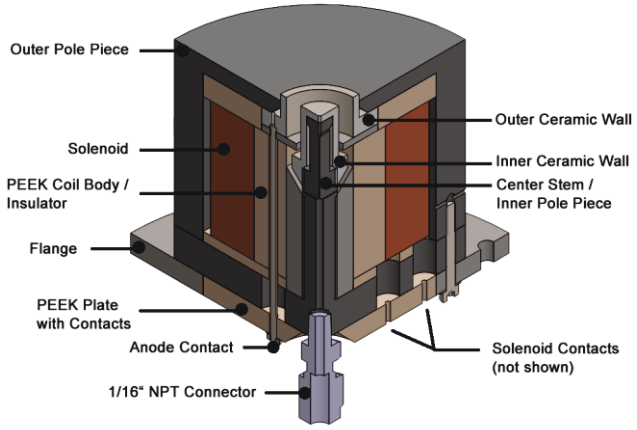

Fig. 14 Sectional View of the Thruster

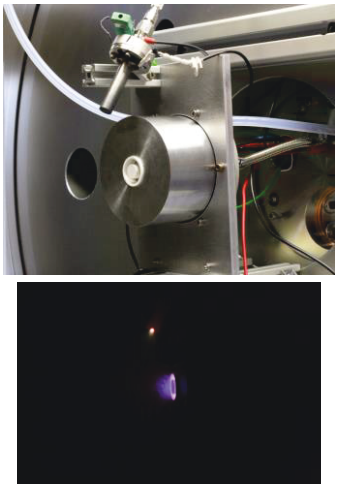

Fig. 15 Hall Thruster and Cathode Mounted and during Operation

The hollow cathode's cathode tube is made out of tantalum. It is clamped to the mounting flange by the boron nitride insulation (see Fig. 15). The insulation also holds the keeper, which is made of molybdenum. The lanthanum hexaboride insert has an inner diameter of 1.3 mm and a length of 6.1 mm, which adds up to an emitting surface of 0.25 cm2. The insert is heated to its operating temperature of 1550 °C by a tungsten heating wire. The wire is wound onto a boron nitride tube, which is slipped over the cathode tube. To avoid direct contact between LaB6 and tantalum, which would cause diffusion of boron into the tantalum material[7], the Insert is wrapped in a graphite film. The cathode is shown in Fig. 16.

2.3.2. Test Results

Both the thruster and the hollow cathode were tested at our lab using Argon as propellant. The thrust over the anode voltage for all magnetic fields is shown in Fig. 17 for a mass flow rate of 0.32 mg/s. All curves in the plot show up a similar course. Analogous to the CVC, higher magnetic fields shift the curves to higher voltage values while the distance between the curves shrinks.

The efficiency over the specific impulse is shown in Fig. 18. Considering the low voltages and the high ionization energy of Argon the conclusion can be drawn that the Argon was ionized only to a small part. Therefore, it is logical that the maximum anode efficiency obtained of about 15% (considering the thrust due to the gas pressure) is very low compared to Xenon thrusters. It can be seen that the efficiency plot with consideration of the thrust due to the gas fits very well between the values from Khayms and Martinez-Sanchez[8] and the values from Komurasaki[9] for higher specific impulse values. This is an indication that the efficiency would rise with higher anode voltage and thus with higher specific impulses.

2.3.3. Future Work

The cathode has shown to be functional, which the successful stable operation and a first characterization shows. Still further improvement regarding the heater setup and the TC fixation is necessary. A future version of the cathode with a C12A7 insert is planned. The Hall effect thruster was successfully tested with argon propellant and a thermionic cathode. Further improvement of the hollow cathode will allow a joint operation. The thruster will also be tested with xenon and further miniaturized with permanent magnets.

a) LaB6 Insert and Graphite Film b) Cathode Tube with Heater Ceramic c) Assembled Hollow Cathode

Fig. 16 Cathode Assembly

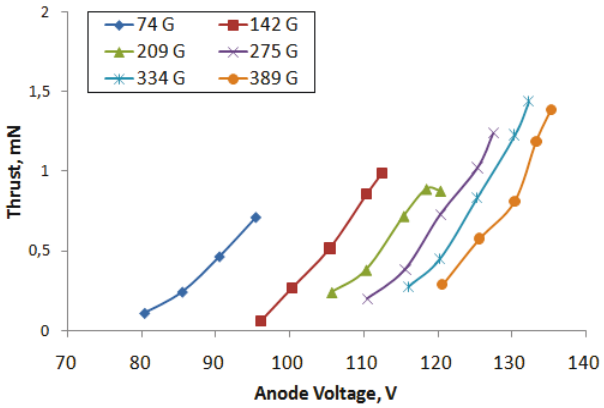

Fig. 17 Thrust versus anode voltage for different magnetic fields at a mass flow rate of 0.32 mg/s

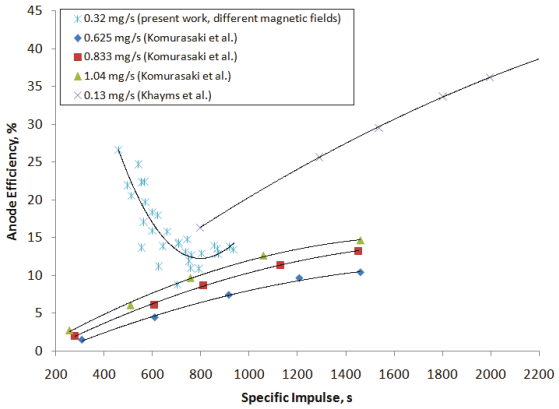

Fig. 18 Comparison of the efficiency data with other Argon-fed Hall thrusters

2.4. Novel Thrust Balance with Nanonewton Thrust Resolution

2.4.1. Basic Setup and Characteristics

Our balance design is similar to other horizontal torsion balances. Such balances allow thrust measurements without the influence of gravity as the measured forces are perpendicular to the weight force. As opposed to this, vertical balances or pendulums always depend on gravity. These are using gravity either by measuring directly the weight force or by using gravity as a reacting force. By using a horizontal balance though, gravitational influences on the measurement result are eliminated. Our balance can handle very small forces with high precision at the same time. The intended measuring range spans from sub-nanonewton ($<10^{-9}$ N) to millinewton (10^{-3} N). The thrust balance is able to operate in high vacuum environment as well as in air.

Our balance design is different with respect to other torsion balances with the following features (summarized in Table 1):

- Thruster weight up to 12 kg possible.
- Balance has electronics package on board to generate high and low voltage (40 kV/100 µA and 10 V/4A) – 24 V bus voltage through bearings without cables.
- Wireless infrared communication with electronics package, temperature sensors and digital I/O
- Passive magnetic damping
- Use of the Philtec mDMS/D64 or attocube FPS interferometric sensor with 1 pm resolution – the best commercially available interferometer.

Fig. 20 shows the working principle and the main parameters of the torsion balance.

The horizontal balance beam is fixed in its middle position with two flexural pivot bearings (from C-Flex Bearing Co. - model G10). These bearings only allow the beam to rotate around the vertical axis and act as a torsion spring with a mostly linear spring rate. The bearings consist of two cylinders connected through thin bending beams without touching each other. By twisting the two cylinders the thin beams are bended which cause the spring properties. Additionally, the used bearings allow a frictionless and lubricant free movement. The total mass of beam, electronics and payload box including the payload is limited by the bearings load capacity to 20 kg.

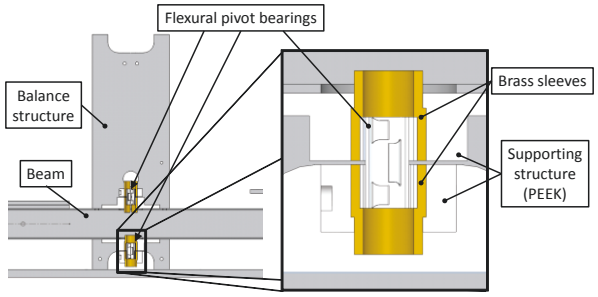

Fig. 19 Cross Section through the Bearings

Fig. 19 shows the bearings implementation of the lower bearing. Two brass sleeves and two PEEK supporting parts are used to attach the two cylinder of the bearing. The upper bearing cylinder is fixed to the beam and the lower one is connected to the balance structure. Due to this design the two bearing cylinders are electrically insulated from each other and to the balance structure. Hence it is possible to provide the total electrical power needed for operating the electronics and the payload through the bearings. With this solution no cables are needed which would influence the overall spring rate of the balance. For controlling the electronics and the payload, wireless infrared communication is used.

The mounted thrust balance is shown in Fig. 21 and Fig. 22.

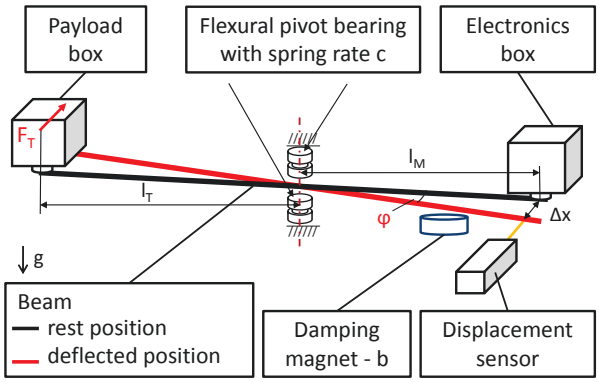

Fig. 20 Schematic Setup of Torsion Balance. The red line illustrates the deflected position (applied thrust) of the beam compared to the black colored rest position (no thrust)

Empty weight Max. thruster weight	8 kg 12 kg
Max. payload power	120 W
Onboard Electronics	40 kV/100 µA, 10 V/4A
Maximum Thrust	6 mN
Resolution of sensors: Philtec Attocube	 2 – 40 nm 1 pm
Min. Thrust Resolution	2.9 pN
Average thrust noise Philtec Attocube	 <1 µN <80 nN

Table 1 Overview of thrust balance characteristics

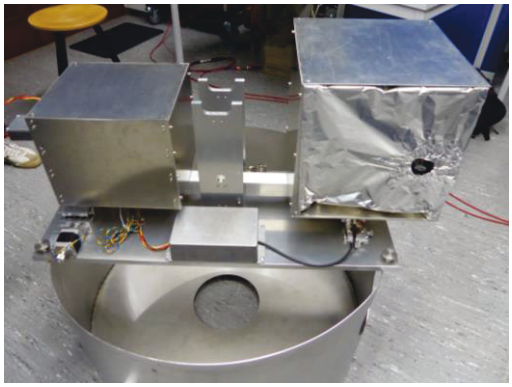

Fig. 21 Horizontal torsion balance equipped with NanoFEEP

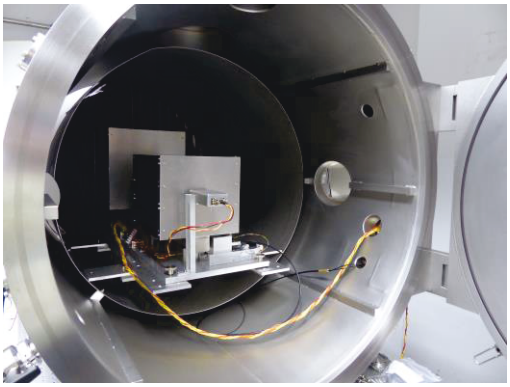

Fig. 22 Torsion balance mounted inside of vacuum chamber an a vibration damping table (not shown)

2.4.2. Thrust Measurement

With applying a horizontal thrust F_T at the distance l_T to the pivot axis a torque is generated which loads the two torsion bearings. The resulting horizontal beam deflection is measured with a displacement sensor located at the distance l_M from the pivot axis. The beam including the payload box and electronics box act like a horizontal torsion pendulum.

In order to rapidly achieve the steady-state position of the beam after applying a certain thrust, an adequate damping system of the beam oscillation is needed. For this purpose a permanent magnet is used. When the beam is oscillating, an eddy current is induced in the conductive beam structure. This eddy current creates its own magnetic field which opposes the magnetic field of the permanent magnet. Thus the relative motion of the beam to the magnet is reduced. With this kind of eddy current brake good damping results of the beam oscillation can be achieve. Knowing the spring rate c (determined by calibration) and the distances l_T and l_M the thrust F_T can be calculated directly from the measured displacement Δx as follows:

$$F_T = \frac{c \cdot \Delta x}{l_T \cdot l_M} \cdot \frac{180°}{\pi} \quad (1)$$

2.4.3. Displacement Sensor

The thrust balance can be equipped with two different displacement sensors to determine the deflection of the balance beam Δx: A fiberoptical displacement sensor (mDMS-64) from Philtec or an interferometric displacement sensor (FPS3010) from attocube.

The fiber optical displacement sensor from Philtec uses bundled glass fibers to emit light to the target and detect the intensity of the reflected light to measure the absolute distance. The measurement range is divided in two distance ranges – the near side and the far side. The near side of the used system ranges from 0 to 300 µm with a resolution of 2 nm and the far side from 300 µm to 6 mm with a resolution of 40 nm. Apart from the resolution, the sensor has noise and drifts in the µm range. For adjustment and changing between near and far side measurement the sensor can be moved by a vacuum-compatible stepper motor.

The interferometric displacement sensor from attocube has a resolution down to only 1 pm and a working distance range up to 400 mm. In this case, no stepper motor is required as there is only one working range which simplifies the setup. The noise at a few Hertz is < 1 nm which is up to three orders of magnitude lower than the Philtec sensor. With signal averaging even lower noise levels are possible towards the pm resolution limit.

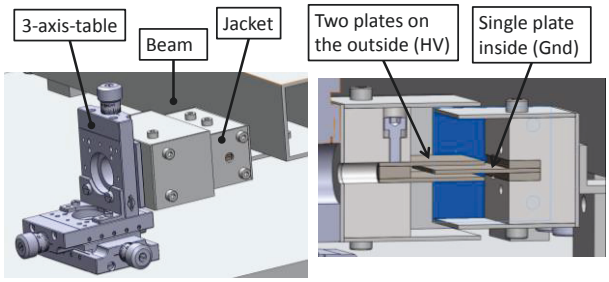

Fig. 23 Electrostatic calibration system and cross section with the double capacitor comb visible

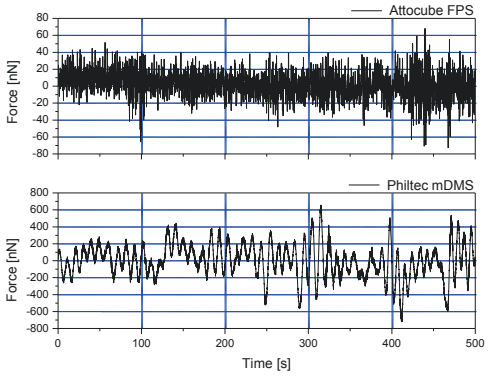

Fig. 24 Noise of balance measured with Philtec and attocube sensor over 500 seconds at a sampling rate of 10 Hz

2.4.4. Calibration of the Balance

To calibrate the balance a defined force is applied to the beam and causes a displacement. The electrostatic comb method shows a way where the calibration force does not dependent on movement of the beam. That is important because the gap between the two electrostatic parts changes if a force is applied and it is fatal if the force would not stay stable. A double plate capacitor is used for this with plates in horizontal position, shown in Fig. 23.

The electrostatic calibration system works like a comb with the smallest amount of couples. The plates on the outside are on adjustable high voltage and is mounted on a three-axis linear stage to adjust the plates as the gap between the plates have to be equal on both sides to prevent vertical forces. The plate in the middle is on ground potential and mounted on the beam. With supplying an electrical potential between the plates a horizontal force F parallel to the plates is generated to the beam.

2.4.5. Noise of Balance

The distance resolution of the fiberoptical sensor mDMS-64 is 2 nm which is equivalent to a maximum force resolution of 5.7 nN. In contrast, the interferometric sensor FPS3010 has a resolution of 1 pm which results in a maximum resolution of 2.89 pN. To compare the noise of both sensors measurements were taken with no applied force. As shown in Fig. 24, the attocube sensor has a noise one order of magnitude better than the Philtec sensor. Better damping should lower the noise even further approaching the sub-Nanolimit regime as we intended. This is one of the lowest thrust noises reported up to date.

Although the thrust balance is working and calibrated, no NanoFEEP test campaign has been carried out yet due to time constraints. Test data will be reported in the near future.

3. BREAKTHROUGH PROPULSION PHYSICS

Present-day propulsion enables robotic exploration of our solar system and manned missions limited to the Earth-Moon distance. With political will and enough resources, there is no doubt that we can develop propulsion technologies that will enable the manned exploration of our solar system.

Unfortunately, present physical limitations and available natural resources do in fact limit human exploration to just that scale. Interstellar travel, even to the next star system Alpha Centauri, is some 4.3 light-years away which is presently inaccessible – on the scale of a human lifetime. For example, one of the fastest manmade objects ever made is the Voyager 1 spacecraft that is presently traveling at a velocity of 0.006% of the speed of light[10]. It will take some 75,000 years for the spacecraft to reach Alpha Centauri.

Although not physically impossible, all interstellar propulsion options are rather mathematical exercises than concepts that could be put into reality in a straightforward manner. For example, from all feasible propulsion systems ever proposed the highest performance is expected from nuclear bombs which are detonated behind the spacecraft (this concept was originally developed under the name Project Orion)[11]. Even such a system would require an order of magnitude more warheads than presently available just to achieve a fly-by mission to our nearest star within a human lifetime.

Even if we could achieve a good fraction of the speed of light, our practical action radius for human-return missions would still be limited to about 10 light-years which includes a maximum of 10 stars around us where no planets have been detected so far. According to the “Maccone Distribution”[12], the next civilization would be most probably some 2000 light-years away which would be inaccessible even with hypothetical light-speed propulsion systems.

It is quite clear that we need some sort of breakthrough in propulsion physics to circumvent these limits and enable practical – and affordable - human exploration well beyond our solar system.

Following the spirit of past programmes such as NASA’s breakthrough propulsion physics and BAE Systems Project Greenglow, we started our own breakthrough propulsion physics program[13] investigating

1. Theory: Explore theoretical concepts that can lead to a practical Space/Warp drive, new approach to

gravity that can be experimentally tested, etc.

2. Mass Modification: Investigate experimentally if mass is influenced by temperature, rotation, charge/polarization, etc.

3. New Gravitational-Like Fields: Carry out experiments to investigate if gravitational/frame-dragging fields can be enhanced in the lab e.g. by strong discharges through superconductors

4. Testing other Claims: Critically assess claims by others on revolutionary propulsion concepts of new physical effects that may lead to a breakthrough in propulsion and/or power

Recent work by our group include a critical evaluation of the EMDrive[14], a replication of the Wallace gravitational generator[15], a superconducting gravitational impulse generator[16] as well as a possible WARP drive concept[17-18] and theoretical work on a connection between electromagnetism, mass and quantum theory[19].

4. ACKNOWLEDGEMENT

We would like to thank attocube (M. Zech) for supplying us the FPS laser interferometer. Part of this work was funded by the German Federal Ministry of Education and Research (BMBF) under contract number 05K2013. The authors are fully responsible for the content of the paper.

5. REFERENCES

[1]Bock, D., Rössler, F., Kössling, M., and Tajmar, M., "Development and Testing of Field Emission Thrusters at TU Dresden", Proceedings of the 5th Russian-German Conference on Electric Propulsion, Dresden, September 7-12 (2014)

[2]Bock, D., Kramer, A., Bangert, P., Schilling, K. and Tajmar, M. "NanoFEEP on UWE platform - Formation Flying of CubeSats using Miniaturized Field Emission Electric Propulsion Thrusters", Proceedings of the 34th International Electric Propulsion Conference, IEPC-2015-121 /ISTS-2015-b-121, Kobe, July 4-10 (2015)

[3]Bock, D., Rössler, F., Kössling, M., and Tajmar, M., "Development and Testing of a CubeSat with Highly Miniaturised FEEP Thrusters on a Thrust Balance with Sub-Nanonewton Resolution", Proceedings of the 65th International Astronautical Congress, Toronto, IAC-14.C4.4.3 (2014)

[4]Bock, D., Bethge, M., and Tajmar, M., "Highly Miniaturized FEEP Thrusters for CubeSat Applications", Proceedings of the 4th Spacecraft Propulsion Conference, Cologne, May 19-22 (2014) 2967498

[5]Tajmar, M. and Stämm, S., "MEMS-Based Gas-Field-Ion-Source for Micro-Thruster and Gas Sensor Application", Proceedings of the 4th Spacecraft Propulsion Conference, Cologne, May 19-22 (2014) 2967499

[6]Nürmberger, F., Hock, A., and Tajmar, M. "Development of a Compact Hall Thruster in the 50-150 Watt Range", 51st AIAA Joint Propulsion Conference, AIAA-2015-3822, Orlando, July 27-29 (2015)

[7]Lafferty, J.M., "Boride Cathodes", Journal of Applied Physics 22(3), 299-309 (1951)

[8]Khayms V. and Martinez-Sanchez, M., "Preliminary experimental evaluation of a miniaturized Hall thruster", IEPC-97-077, 25th International Electric Propulsion Conference (1997)

[9]Komurasaki, K., Hirakawa, M., and Arakawa, Y. "Plasma Acceleration Process in a Hall Thruster", IEPC-91-078, 22rd International Electric Propulsion Conference (1991)

[10]Frisbee R. H., "Advanced Propulsion for the 21st Century", Journal of Propulsion and Power 19(6), 1129-1154 (2003)

[11]Tajmar M., "Advanced Space Propulsion Systems", Springer, 2003

[12]Maccone, C., "The Statistical Drake Equation", 59th International Astronautical Congress, Glasgow, Scotland, GB, Paper IAC-08-A4.1.4 (2008)

[13]http://www.tu-dresden.de/ilr/rfs/bpp

[14]Tajmar, M. and Fiedler, G., "Direct Thrust Measurements of an EMDrive and Evaluation of Possible Side-Effects", 51st AIAA Joint Propulsion Conference, AIAA-2015-4083, Orlando, July 27-29 (2015)

[15]Boy, C., Lörincz, I., and Tajmar, M., "Replication and Experimental Characterization of the Wallace Dynamic Force Field Generator", 51st AIAA Joint Propulsion Conference, AIAA-2015-4081, Orlando, July 27-29 (2015)

[16]Lörincz, I. and Tajmar, M., "Design and First Measurements of a Superconducting Gravity-Impulse-Generator", 51st AIAA Joint Propulsion Conference, AIAA-2015-4080, Orlando, July 27-29 (2015)

[17]Tajmar, M., "Propellantless Propulsion with Negative Matter Generated by Electric Charges", AIAA Joint Propulsion Conference, AIAA-2013-3913, 2013

[18]Tajmar, M., and Assis, A.K.T., "Particles with Negative Mass: Production, Properties and Applications for Nuclear Fusion and Self-Acceleration", Journal of Advanced Physics 4, 77-82 (2015)

[19]Tajmar, M., "Derivation of the Planck and Fine-Structure Constant from Assis's Gravity Model", Journal of Advanced Physics 4, 219-221 (2015)